Supporting Information for the Manuscript

Syntheses and fluorescence properties of lanthanide isostructural complexes derived from aspartic acid

Yatong Zhang,[a] Ai Wang, *[a,b] Sisi Feng,[a,b] Caixia Yuan,[a] Liping Lu *[a]

[a] Institute of Molecular Science, Key Laboratory of Chemical Biology and Molecular Engineering of the Education Ministry, Shanxi University, Taiyuan, Shanxi 030006, People's Republic of China.

[b] Key Laboratory of Materials for Energy Conversion and Storage of Shanxi Province; Shanxi University, Taiyuan, Shanxi 030006, People's Republic of China.

*Corresponding authors, E-mail: aiwang@sxu.edu.cn; luliping@sxu.edu.cn.

Content

S1 Experiment content

S1.1 Materials and physical measurements

The N-(4-carboxylbenzyl)-L-aspartic acid (H_3caa) was used as the ligand in this work and purchased from Jinan Trading Company, China. Other chemicals and solvents were reagent grade and purchased directly without secondary treatment. Element analysis (CHN) was performed using a PerkinElmer 240 elemental analyzer. Samples' infra-red spectra were recorded on a Bruker TENSOR27 spectrometer with KBr pellets in the range of 4000 − 400 cm^{-1}. The power X-ray diffraction (PXRD) patterns were recorded by using a Bruker D8 Advance X-ray Diffractometer with Cu $K\alpha$ radiation at a scan speed of 5 $^{o}\cdot min^{-1}$ in the range of 2θ = 5 – 50 º. The thermos-gravi-metric analysis (TGA) data of complexes **1** − **6** was carried out on a DuPont thermal analyzer from room temperature to 860ºC under an air atmosphere with the heating rate of 10ºC·min^{-1}. Room temperature fluorescence spectra and the photoluminescence quantum yield were obtained by using an Edinburge FS5 Spectrofluorometer with a xenon arc lamp as the light source. The UV-Vis absorption spectra were obtained *via* a Hewlett Packard HP-8453 UV absorption spectrometer.

S1.2 X-ray crystallographic analyses

The single-crystal X-ray diffraction data for complexes **1** − **6** were collected on a Bruker D8-Quest diffractometer equipped with a Photon 100 detector by using graphite-monochromated Mo-$K\alpha$ radiation (λ = 0.71073 Å) at normal temperature. The program SADABS was used for absorption corrections [S1]. The crystal structures were solved by direct methods and refined by full-matrix least-squares methods

against F^2 with SHELX-2014 program [S2]. All non-hydrogen atoms were refined anisotropically and refined using a riding model approximation. Hydrogen atoms attached to C atoms were placed geometrically and refined using a riding model approximation, with C(sp^2) − H = 0.93 Å and U_{iso}(H) = 1.2U_{eq}(C). The H atoms bonded to O atoms were assigned isotropic displacement parameters U_{iso}(H) = 1.5U_{eq}(O). The H atoms bonded to N atoms were assigned isotropic displacement parameters U_{iso}(H) = 1.2U_{eq}(N). The structure refinement details, crystallographic data and data collection are provided in Table S1. Some chosen bond lengths, angles and hydrogen bonds information are listed in Tables S2 and S3.

S1.3 Fluorescence detection experiment

Photoluminescence (PL) measurements were carried out using complex **6**. The aqueous suspension was prepared by grinding 5.0 mg complex **6** into 50.00 mL aqueous solution (~ 0.1 g/L), ultrasonic treatment for 30 min, and then aging for 2 days which were filtered by using 0.22 μm filter membranes to form a transparent suspension before fluorescence detection experiment. By adding 200 μL different ions (0.1 mmol/L, as K^+, Na^+, Mg^{2+}, Ca^{2+}, Ba^{2+}, Mn^{2+}, Co^{2+}, Ni^{2+}, Zn^{2+}, Cd^{2+}, Cr^{3+}, Ga^{3+}, Al^{3+}, Ce^{3+}, Dy^{3+}, Gd^{3+}, La^{3+}, Nd^{3+}, Eu^{3+}, Pr^{3+}, Ho^{3+}, Sm^{3+}, Er^{3+}, Tb^{3+}, Cl^-, Br^-, I^-, $C_2O_4^{2-}$, CO_3^{2-}, NO_3^-, OH^-, HPO_4^{2-}, SO_4^{2-}, $H_2PO_4^-$, CH_3COO^- and HCO_3^-) or different biomolecules [0.1 mmol/L, such as Ibuprofen (IBU), Gemfibrozil (GEM), Sulfamethoxazole (SMZ), Trimethoprim (TMP), Diclofenac (DCF), Ornidazole (ORN), 4-Acetamidophenol (APAP), Chlorotetracycline hydrochloride (CTC), Tetracycline hydrochloride (TC), Glycine (Gly), Isoleucine (Ile), Proline (Pro), Valine

(Val), Alanine (Ala), Serine (Ser), Methionine (Met), Glutamic acid (Glu), Histidine (His), Threonine (Thr), Aspartic acid (Asp), Leucine (Leu), Argnine (Arg), Phenylalanine (Phe), Lysine (Lys), Tyrosine (Tyr), Cysteine (Cys) and Ascorbic acid (AA)] into 2.0 mL complex **6** aqueous suspension enable the detection of different ions to be completed. The fluorescence sensing properties of complex **6** to $Cr_2O_7^{2-}$, CrO_4^{2-}, CTC and TC were further explored by collecting emission spectra of 0.1 mmol/L $Cr_2O_7^{2-}$, CrO_4^{2-}, CTC and TC ions (0 ~ 200 μL) in complex **6** aqueous suspension.

S1.4 Fluorescent test strips test

Filter papers with the size of 5 × 0.5 cm^2 were soaked in the aqueous suspension of complex **6** for 30 minutes, and then the filter paper strip was taken out and dried in an oven at 70°C for 1 hour to form the fluorescent strips of complex **6**. Then the strips were immersed in different ions or biomolecules with different concentrations for 1 min.

S1.5 Fluorescent sensing film

Weigh 200 mg of agar powder and 50 mg of complex **6** into a 25 mL beaker, and then add 10 mL of distilled water. After heating it at 90ºC for 10 min, and taking 1 mL of it in a mold of 3 × 3 × 0.3 cm^3, and then standing for 10 min to form a fluorescent sensing film.

S1.6 Fluorescence quantum yield measurements

The SC-30 integrating sphere module is used for the measurement of absolute photoluminescence quantum yields [S3]. For the measurement of solid samples, the blank device that comes with the instrument. Firstly, xenon lamp and red PMT-900

Sphere were chose as the source light path and detector light path. Secondly, the emission scan setup was same as that of the standard procedure of solid-state fluorescence emission spectra. Then the fluorescence emission spectrum of blank was recorded under excitation wavelength of sample. Herein, the excitation wavelength is 294 nm. The solid sample for **6** and recovered **6** after immersion with Cr(VI) and TCs were dried fully. Then, 2 mg of fully ground solid samples were put in sample cell and recorded the data. For the quantum yield calculation, the ‘direct only’ was selected to be the measurements type and ‘standard analysis’ was chose as the analysis type.

Table S1 Crystal data and structure refinement for complexes **1 − 6**

Complex	**1**	**2**	**3**	**4**	**5**	**6**
CCDC	2236703	2236704	2236705	2236706	2236707	2236708
Formula	$C_{12}H_{13}CeClNO_7$	$C_{12}H_{13}ClNO_7Pr$	$C_{12}H_{13}ClNNdO_7$	$C_{12}H_{13}ClNO_7Sm$	$C_{12}H_{13}ClEuNO_7$	$C_{12}H_{13}ClNO_7Tb$
Formula weight	458.80	459.59	462.92	469.03	470.64	477.60
Crystal system	Monoclinic	Monoclinic	Monoclinic	Monoclinic	Monoclinic	Monoclinic
Space group	$P2_1/c$	$P2_1/c$	$P2_1/c$	$P2_1/c$	$P2_1/c$	$P2_1/c$
T / K	298 (2)	298 (2)	298 (2)	298 (2)	298 (2)	298 (2)
***a* / Å**	14.424 (5)	14.368 (19)	14.441 (6)	14.3665 (16)	14.365 (4)	14.365 (6)
***b* / Å**	12.494 (4)	12.445 (18)	12.511 (5)	12.3921 (13)	12.400 (4)	12.378 (5)
***c* / Å**	8.027 (3)	7.961 (14)	7.996 (3)	7.8827 (8)	7.874 (2)	7.859 (3)
***β* / º**	95.411 (8)	95.443(5)	95.595 (10)	95.556 (3)	95.572 (8)	95.858 (11)
***V* / Å^3**	1440.1 (9)	1417.1 (4)	1437.8 (10)	1396.8 (3)	1395.9 (7)	1390.0 (9)
Z	4	4	4	4	4	4
***F* (000)**	892	896	900	908	912	920
Goof	1.02	1.03	1.05	1.03	1.03	1.07
R_1	0.035	0.037	0.069	0.028	0.043	0.058
ωR_2	0.089	0.081	0.166	0.068	0.107	0.135

Table S2 Selected bond lengths (Å) and bond angles (º) for complexes **1 − 6**

Complex **1**					
Bond	**Dist. (Å)**	**Bond**	**Dist. (Å)**	**Bond**	**Dist. (Å)**

Ce1—O1	2.452 (4)	Ce1—O7	2.520 (3)	Ce1—O3^{v}	2.582 (4)
Ce1—O6^{i}	2.470 (3)	Ce1—O5^{iii}	2.526 (4)	Ce1—O4^{v}	2.611 (4)
Ce1—O4^{ii}	2.489 (3)	Ce1—O2^{iv}	2.550 (4)	Ce1—O5^{i}	2.722 (4)
Ce1···Ce1^{vi}	4.196 (1)				
Angle	**(º)**	**Angle**	**(º)**	**Angle**	**(º)**
O1—Ce1—O6^{i}	75.15 (13)	O1—Ce1—O2^{iv}	140.83 (13)	O2^{iv}—Ce1—O3^{v}	109.91 (14)
O1—Ce1—O4^{ii}	141.36 (13)	O6^{i}—Ce1—O2^{iv}	112.50 (13)	O1—Ce1—O4^{v}	73.22 (12)
O6^{i}—Ce1—O4^{ii}	115.02 (12)	O4^{ii}—Ce1—O2^{iv}	72.56 (12)	O6^{i}—Ce1—O4^{v}	141.12 (11)
O1—Ce1—O7	75.82 (14)	O7—Ce1—O2^{iv}	143.28 (13)	O4^{ii}—Ce1—O4^{v}	103.80 (11)
O6^{i}—Ce1—O7	72.58 (13)	O5^{iii}—Ce1—O2^{iv}	71.99 (12)	O7—Ce1—O4^{v}	119.65 (12)
O4^{ii}—Ce1—O7	72.74 (13)	O1—Ce1—O3^{v}	73.75 (15)	O5^{iii}—Ce1—O4^{v}	71.75 (11)
O1—Ce1—O5^{iii}	72.58 (13)	O6^{i}—Ce1—O3^{v}	137.52 (14)	O2^{iv}—Ce1—O4^{v}	80.30 (12)
O6^{i}—Ce1—O5^{iii}	77.67 (12)	O4^{ii}—Ce1—O3^{v}	75.69 (13)	O3^{v}—Ce1—O4^{v}	49.91 (12)
O4^{ii}—Ce1—O5^{iii}	144.50 (12)	O7—Ce1—O3^{v}	72.27 (13)	O1—Ce1—O5^{i}	123.74 (12)
O7—Ce1—O5^{iii}	141.00 (12)	O5^{iii}—Ce1—O3^{v}	118.56 (12)	O6^{i}—Ce1—O5^{i}	49.64 (11)

Symmetry codes: (i) -*x*+1, -*y*+1, -*z*+2; (ii) -*x*, *y*+1/2, -*z*+3/2; (iii) -*x*+1, *y*+1/2, -*z*+3/2; (iv) *x*, -*y*+3/2, *z*+1/2; (v) -*x*, -*y*+1, -*z*+1, (vi) *x*, -*y*+3/2, *z*-1/2

Complex **2**

Bond	**Å**	**Bond**	**Å**	**Bond**	**Å**
Pr1—O1	2.429 (4)	Pr1—O7	2.498 (4)	Pr1—O3^{v}	2.560 (4)
Pr1—O6^{i}	2.444 (4)	Pr1—O5^{iii}	2.503 (4)	Pr1—O4^{v}	2.579 (4)
Pr1—O4^{ii}	2.469 (3)	Pr1—O2^{iv}	2.531 (4)	Pr1—O5^{i}	2.698 (4)
Pr1···Pr1^{vi}	4.162 (8)				
Angle	**(º)**	**Angle**	**(º)**	**Angle**	**(º)**
O1—Pr1—O6^{i}	74.72 (14)	O1—Pr1—O2^{iv}	141.33 (13)	O2^{iv}—Pr1—O3^{v}	110.14 (15)
O1—Pr1—O4^{ii}	141.09 (13)	O6^{i}—Pr1—O2^{iv}	112.46 (13)	O1—Pr1—O4^{v}	73.64 (13)

O6^{i}—Pr1—O4^{ii}	115.04 (12)	O4^{ii}—Pr1—O2^{iv}	72.62 (12)	O6^{i}—Pr1—O4^{v}	140.81 (12)
O1—Pr1—O7	75.50 (14)	O7—Pr1—O2^{iv}	143.11 (13)	O4^{ii}—Pr1—O4^{v}	104.10 (12)
O6^{i}—Pr1—O7	72.69 (13)	O5^{iii}—Pr1—O2^{iv}	72.23 (12)	O7—Pr1—O4^{v}	119.91 (13)
O4^{ii}—Pr1—O7	72.52 (13)	O1—Pr1—O3^{v}	73.75 (16)	O5^{iii}—Pr1—O4^{v}	71.63 (11)
O1—Pr1—O5^{iii}	72.72 (13)	O6^{i}—Pr1—O3^{v}	137.34 (15)	O2^{iv}—Pr1—O4^{v}	80.27 (12)
O6^{i}—Pr1—O5^{iii}	77.34 (12)	O4^{ii}—Pr1—O3^{v}	75.77 (13)	O3^{v}—Pr1—O4^{v}	50.28 (12)
O4^{ii}—Pr1—O5^{iii}	144.79 (12)	O7—Pr1—O3^{v}	72.13 (14)	O1—Pr1—O5^{i}	123.70 (12)
O7—Pr1—O5^{iii}	140.86 (13)	O5^{iii}—Pr1—O3^{v}	118.70 (13)	O6^{i}—Pr1—O5^{i}	50.09 (11)

Symmetry codes: (i) -*x*+1, -*y*+1, -*z*+2; (ii) -*x*, *y*+1/2, -*z*+3/2; (iii) -*x*+1, *y*+1/2, -*z*+3/2; (iv) *x*, -*y*+3/2, *z*+1/2; (v) -*x*, -*y*+1, -*z*+1, (vi) *x*, -*y*+3/2, *z*-1/2

Complex **3**

Bond	**Å**	**Bond**	**Å**	**Bond**	**Å**
Nd1—O1	2.426 (9)	Nd1—O7	2.495 (9)	Nd1—O3^{v}	2.566 (9)
Nd1—O6^{i}	2.449 (8)	Nd1—O5^{iii}	2.518 (9)	Nd1—O4^{v}	2.586 (8)
Nd1—O4^{ii}	2.476 (9)	Nd1—O2^{iv}	2.542 (9)	Nd1—O5^{i}	2.709 (9)
Nd1···Nd1^{vi}	4.179 (2)				
Angle	**(º)**	**Angle**	**(º)**	**Angle**	**(º)**
O1—Nd1—O6^{i}	74.6 (3)	O1—Nd1—O2^{iv}	141.8 (3)	O2^{iv}—Nd1—O3^{v}	110.5 (3)
O1—Nd1—O4^{ii}	140.8 (3)	O6^{i}—Nd1—O2^{iv}	112.1 (3)	O1—Nd1—O4^{v}	73.8 (3)
O6^{i}—Nd1—O4^{ii}	114.8 (3)	O4^{ii}—Nd1—O2^{iv}	72.7 (3)	O6^{i}—Nd1—O4^{v}	140.8 (3)
O1—Nd1—O7	75.5 (3)	O7—Nd1—O2^{iv}	142.7 (3)	O4^{ii}—Nd1—O4^{v}	104.3 (3)
O6^{i}—Nd1—O7	73.0 (3)	O5^{iii}—Nd1—O2^{iv}	72.5 (3)	O7—Nd1—O4^{v}	119.8 (3)
O4^{ii}—Nd1—O7	72.0 (3)	O1—Nd1—O3^{v}	73.7 (3)	O5^{iii}—Nd1—O4^{v}	71.6 (3)
O1—Nd1—O5^{iii}	72.6 (3)	O6^{i}—Nd1—O3^{v}	137.3 (3)	O2^{iv}—Nd1—O4^{v}	80.7 (3)
O6^{i}—Nd1—O5^{iii}	77.3 (3)	O4^{ii}—Nd1—O3^{v}	75.9 (3)	O3^{v}—Nd1—O4^{v}	50.3 (3)
O4^{ii}—Nd1—O5^{iii}	145.3 (3)	O7—Nd1—O3^{v}	72.0 (3)	O1—Nd1—O5^{i}	123.6 (3)

O7—Nd1—O5^{iii}	140.9 (3)	O5^{iii}—Nd1—O3^{v}	118.5 (3)	O6^{i}—Nd1—O5^{i}	50.1 (3)

Symmetry codes: (i) -*x*+1, -*y*+1, -*z*+2; (ii) -*x*, *y*+1/2, -*z*+3/2; (iii) -*x*+1, *y*+1/2, -*z*+3/2; (iv) *x*, -*y*+3/2, *z*+1/2; (v) -*x*, -*y*+1, -*z*+1, (vi) *x*, -*y*+3/2, *z*-1/2

Complex **4**

Bond	**Dist. (Å)**	**Bond**	**Dist. (Å)**	**Bond**	**Dist. (Å)**
Sm1—O1	2.387 (3)	Sm1—O7	2.449 (3)	Sm1—O3^{v}	2.515 (3)
Sm1—O6^{i}	2.405 (3)	Sm1—O5^{iii}	2.468 (3)	Sm1—O4^{v}	2.540 (3)
Sm1—O4^{ii}	2.433 (3)	Sm1—O2^{iv}	2.480 (3)	Sm1—O5^{i}	2.675 (3)
Sm1···Sm1^{vi}	4.122 (5)				
Angle	**(º)**	**Angle**	**(º)**	**Angle**	**(º)**
O1—Sm1—O6^{i}	74.62 (11)	O1—Sm1—O2^{iv}	141.50 (11)	O2^{iv}—Sm1—O3^{v}	110.46 (12)
O1—Sm1—O4^{ii}	140.98 (11)	O6^{i}—Sm1—O2^{iv}	112.22 (11)	O1—Sm1—O4^{v}	73.80 (10)
O6^{i}—Sm1—O4^{ii}	114.83 (10)	O4^{ii}—Sm1—O2^{iv}	72.81 (10)	O6^{i}—Sm1—O4^{v}	140.33 (10)
O1—Sm1—O7	75.56 (11)	O7—Sm1—O2^{iv}	142.89 (11)	O4^{ii}—Sm1—O4^{v}	104.82 (9)
O6^{i}—Sm1—O7	73.03 (11)	O5^{iii}—Sm1—O2^{iv}	72.26 (11)	O7—Sm1—O4^{v}	120.45 (10)
O4^{ii}—Sm1—O7	72.06 (10)	O1—Sm1—O3^{v}	73.68 (13)	O5^{iii}—Sm1—O4^{v}	71.25 (10)
O1—Sm1—O5^{iii}	72.82 (11)	O6^{i}—Sm1—O3^{v}	137.26 (13)	O2^{iv}—Sm1—O4^{v}	80.07 (10)
O6^{i}—Sm1—O5^{iii}	76.96 (11)	O4^{ii}—Sm1—O3^{v}	75.98 (11)	O3^{v}—Sm1—O4^{v}	51.06 (10)
O4^{ii}—Sm1—O5^{iii}	145.00 (11)	O7—Sm1—O3^{v}	71.85 (11)	O1—Sm1—O5^{i}	123.98 (10)
O7—Sm1—O5^{iii}	140.96 (11)	O5^{iii}—Sm1—O3^{v}	118.98 (11)	O6^{i}—Sm1—O5^{i}	50.55 (10)

Symmetry codes: (i) -*x*+1, -*y*+1, -*z*+2; (ii) -*x*, *y*+1/2, -*z*+3/2; (iii) -*x*+1, *y*+1/2, -*z*+3/2; (iv) *x*, -*y*+3/2, *z*+1/2; (v) -*x*, -*y*+1, -*z*+1, (vi) *x*, -*y*+3/2, *z*-1/2

Complex **5**

Bond	**Dist. (Å)**	**Bond**	**Dist. (Å)**	**Bond**	**Dist. (Å)**
Eu1—O1	2.376 (5)	Eu1—O7	2.441 (5)	Eu1—O3^{v}	2.510 (6)
Eu1—O6^{i}	2.394 (5)	Eu1—O5^{iii}	2.461 (6)	Eu1—O4^{v}	2.546 (5)

Eu1—O4^{ii}	2.417 (5)	Eu1—O2^{iv}	2.468 (6)	Eu1—O5^{i}	2.678 (6)
Eu1···Eu1^{vi}	4.117 (1)				
Angle	**(º)**	**Angle**	**(º)**	**Angle**	**(º)**
O1—Eu1—O6^{i}	74.6 (2)	O1—Eu1—O2^{iv}	141.76 (19)	O2^{iv}—Eu1—O3^{v}	110.9 (2)
O1—Eu1—O4^{ii}	140.7 (19)	O6^{i}—Eu1—O2^{iv}	111.9 (2)	O1—Eu1—O4^{v}	73.70 (18)
O6^{i}—Eu1—O4^{ii}	114.91 (18)	O4^{ii}—Eu1—O2^{iv}	72.82 (17)	O6^{i}—Eu1—O4^{v}	140.12 (18)
O1—Eu1—O7	75.5 (2)	O7—Eu1—O2^{iv}	142.67 (18)	O4^{ii}—Eu1—O4^{v}	104.94 (16)
O6^{i}—Eu1—O7	73.25 (19)	O5^{iii}—Eu1—O2^{iv}	72.03 (18)	O7—Eu1—O4^{v}	120.44 (18)
O4^{ii}—Eu1—O7	71.88 (18)	O1—Eu1—O3^{v}	73.4 (2)	O5^{iii}—Eu1—O4^{v}	71.07 (17)
O1—Eu1—O5^{iii}	73.21 (19)	O6^{i}—Eu1—O3^{v}	137.1 (2)	O2^{iv}—Eu1—O4^{v}	80.36 (18)
O6^{i}—Eu1—O5^{iii}	77.01 (19)	O4^{ii}—Eu1—O3^{v}	76.0 (2)	O3^{v}—Eu1—O4^{v}	51.30 (18)
O4^{ii}—Eu1—O5^{iii}	144.79 (18)	O7—Eu1—O3^{v}	71.6 (2)	O1—Eu1—O5^{i}	123.96 (17)
O7—Eu1—O5^{iii}	141.36 (19)	O5^{iii}—Eu1—O3^{v}	119.09 (19)	O6^{i}—Eu1—O5^{i}	50.55 (18)

Symmetry codes: (i) -*x*+1, -*y*+1, -*z*+2; (ii) -*x*, *y*+1/2, -*z*+3/2; (iii) -*x*+1, *y*+1/2, -*z*+3/2; (iv) *x*, -*y*+3/2, *z*+1/2; (v) -*x*, -*y*+1, -*z*+1, (vi) *x*, -*y*+3/2, *z*-1/2

Complex **6**

Bond	**Dist. (Å)**	**Bond**	**Dist. (Å)**	**Bond**	**Dist. (Å)**
Tb1—O1	2.358 (9)	Tb1—O4^{ii}	2.422 (9)	Tb1—O3^{v}	2.478 (10)
Tb1—O6^{i}	2.358 (10)	Tb1—O5^{iii}	2.440 (10)	Tb1—O4^{v}	2.526 (9)
Tb1—O7	2.415 (9)	Tb1—O2^{iv}	2.445 (9)	Tb1—O5^{i}	2.696 (10)
Tb1···Tb1^{vi}	4.110 (2)				
Angle	**(º)**	**Angle**	**(º)**	**Angle**	**(º)**
O1—Tb1—O6^{i}	74.5 (3)	O1—Tb1—O2^{iv}	141.7 (3)	O2^{iv}—Tb1—O3^{v}	111.0 (4)
O1—Tb1—O7	76.2 (3)	O6^{i}—Tb1—O2^{iv}	111.9 (4)	O1—Tb1—O4^{v}	73.9 (3)
O6^{i}—Tb1—O7	73.3 (3)	O7—Tb1—O2^{iv}	142.1 (3)	O6^{i}—Tb1—O4^{v}	140.3 (3)
O1—Tb1—O4^{ii}	141.1 (3)	O4^{ii}—Tb1—O2^{iv}	72.8 (3)	O7—Tb1—O4^{v}	120.8 (3)

O6^{i}—Tb1—O4^{ii}	114.5 (3)	O5^{iii}—Tb1—O2^{iv}	72.5 (3)	O4^{ii}—Tb1—O4^{v}	105.2 (3)
O7—Tb1—O4^{ii}	71.3 (3)	O1—Tb1—O3^{v}	73.5 (4)	O5^{iii}—Tb1—O4^{v}	71.6 (3)
O1—Tb1—O5^{iii}	72.8 (3)	O6^{i}—Tb1—O3^{v}	137.0 (4)	O2^{iv}—Tb1—O4^{v}	80.4 (3)
O6^{i}—Tb1—O5^{iii}	76.5 (3)	O7—Tb1—O3^{v}	71.8 (3)	O3^{v}—Tb1—O4^{v}	51.2 (3)
O7—Tb1—O5^{iii}	141.2 (3)	O4^{ii}—Tb1—O3^{v}	76.4 (3)	O1—Tb1—O5^{i}	124.4 (3)
O4^{ii}—Tb1—O5^{iii}	145.2 (3)	O5^{iii}—Tb1—O3^{v}	119.3 (3)	O6^{i}—Tb1—O5^{i}	51.0 (3)

Symmetry codes: (i) -*x*+1, -*y*+1, -*z*+2; (ii) -*x*, *y*+1/2, -*z*+3/2; (iii) -*x*+1, *y*+1/2, -*z*+3/2; (iv) *x*, -*y*+3/2, *z*+1/2; (v) -*x*, -*y*+1, -*z*+1, (vi) *x*, -*y*+3/2, *z*-1/2

Table S3 Weak interaction (Å and º) for complexes **1 − 6**

Complex **1**

D—H···A	D—H	H···A	D···A	D—H···A
O7—H7B···O3^{ix}	0.83	2.36	3.101 (5)	149
O7—H7B···O2^{ix}	0.83	2.59	3.106 (6)	122
O7—H7A···Cl1^{x}	0.83	2.57	3.193 (4)	133
N1—H1B···Cl1	0.89	2.20	3.063 (4)	163
N1—H1A···Cl1^{x}	0.89	2.44	3.252 (5)	153

Symmetry codes: (ix) *x*, *y*, *z*+1; (x) *x*, -*y*+1/2, *z*+1/2.

Complex **2**

D—H···A	D—H	H···A	D···A	D—H···A
O7—H7B···O2^{x}	0.83	2.57	3.078 (6)	122
O7—H7B···O3^{x}	0.83	2.36	3.089 (5)	148
O7—H7A···Cl1^{ix}	0.82	2.55	3.175 (4)	133
N1—H1B···Cl1	0.89	2.20	3.060 (4)	163
N1—H1A···Cl1^{ix}	0.89	2.43	3.242 (5)	153

Symmetry codes: (ix) *x*, -*y*+1/2, *z*+1/2; (x) *x*, *y*, *z*+1.

Complex **3**

D—H···A	D—H	H···A	D···A	D—H···A
O7—H7B···O3^{ix}	0.83	2.40	3.136 (13)	148
O7—H7B···O2^{ix}	0.83	2.60	3.113 (13)	122
O7—H7A···Cl1^{x}	0.83	2.59	3.213 (10)	133
N1—H1A···Cl1	0.89	2.21	3.074 (11)	165
N1—H1B···Cl1^{x}	0.89	2.44	3.263 (12)	154

Symmetry codes: (ix) *x*, *y*, *z*+1; (x) *x*, -*y*+1/2, *z*+1/2.

Complex **4**

D—H···A	D—H	H···A	D···A	D—H···A
O7—H7B···O3^{x}	0.82	2.39	3.105 (5)	147
O7—H7B···O2^{x}	0.82	2.53	3.039 (5)	121
O7—H7A···Cl1^{ix}	0.82	2.56	3.175 (4)	133
N1—H1B···Cl1	0.89	2.19	3.058 (3)	164
N1—H1A···Cl1^{ix}	0.89	2.41	3.226 (4)	152

Symmetry codes: (ix) *x*, -*y*+1/2, *z*+1/2; (x) *x*, *y*, *z*+1.

Complex **5**

D—H···A	D—H	H···A	D···A	D—H···A
O7—H7B···O3^{i}	0.82	2.39	3.105 (8)	147
O7—H7B···O2^{i}	0.82	2.55	3.051 (8)	121
O7—H7A···Cl1^{ii}	0.82	2.57	3.182 (6)	133
N1—H1B···Cl1	0.89	2.20	3.064 (6)	164
N1—H1A···Cl1^{ii}	0.89	2.42	3.235 (7)	153

Symmetry codes: (i) *x*, *y*, *z*+1; (ii) *x*, -*y*+1/2, *z*+1/2.

Complex **6**

D—H···A	D—H	H···A	D···A	D—H···A
O7—H7B···O3^{ix}	0.82	2.42	3.131 (13)	146
O7—H7B···O2^{ix}	0.82	2.54	3.046 (12)	121
O7—H7A···Cl1^{x}	0.82	2.57	3.189 (10)	133
N1—H1A···Cl1	0.89	2.21	3.080 (10)	164

N1—H1B···Cl1^{x}	0.89	2.42	3.237 (10)	153

Symmetry codes: (ix) *x*, *y*, *z*+1; (x) *x*, -*y*+1/2, *z*+1/2.

Table S4 Quantum yield results of complexes **1** − **6**

Sample	**1** (440 nm)	**2** (420 nm)	**3** (420 nm)
Quantum yield	0.1%	0.4%	0.4%
Sample	**4** (428 nm)	**5** (613 nm)	**6** (543 nm)
Quantum yield	0.8%	10.1%	31.7%

Table S5 Comparison of various complex sensors for detecting $Cr_2O_7^{2-}$, CrO_4^{2-}, CTC or TC

No.	Complex	Analyte	Detection range	LOD	Media	Ref.
1	**Complex 6**	**$Cr_2O_7^{2-}$**	**0–0.95 μM**	**3.66 nM**	**H_2O**	**This work**
2	HBU-20	$Cr_2O_7^{2-}$	--	8.9 nM	H_2O	S4
3	$\{Tb(cpon)(Hcpon)(H_2O)_3\}_n$	$Cr_2O_7^{2-}$	0–100 μM	0.25 μM	H_2O	S5
4	$Tb_{0.5}Y_{0.5}$-MOF	$Cr_2O_7^{2-}$	1–1000 μM	0.36 μM	H_2O	S6
5	$[Tb_2(pyia)_3(phen)_2(H_2O)]\cdot H_2O$	$Cr_2O_7^{2-}$	--	0.53 μM	H_2O	S7
6	$Eu_{0.075}Tb_{0.925}$-MOF	$Cr_2O_7^{2-}$	10–100 μM	0.872 μM	H_2O	S8
7	$\{[Tb(L)(DMF)(H_2O)]\}_n$	$Cr_2O_7^{2-}$	--	1.14 μM	DMF	S9
8	UiO-66-NH-BT	$Cr_2O_7^{2-}$	--	1.3 μM	H_2O	S10
9	$[Tb(L)(HCOO)(H_2O)]_n$	$Cr_2O_7^{2-}$	--	2.1 μM	H_2O	S11
10	USTS-7	$Cr_2O_7^{2-}$	0.01–0.5 μM	2.2 μM	DMF	S12
11	CUST-604	$Cr_2O_7^{2-}$	100–250 μM	2.29 μM	DMF	S13
12	$[Zn_3Eu_2(TTHA)_2(H_2O)_6]\cdot 6H_2O$	$Cr_2O_7^{2-}$	0–260 μM	3.00 μM	EtOH	S14
13	CUST-603	$Cr_2O_7^{2-}$	0–300 μM	3.86 μM	DMF	S13
14	CUST-602	$Cr_2O_7^{2-}$	0–250 μM	5.86 μM	DMF	S13
15	CUST-601	$Cr_2O_7^{2-}$	60–300 μM	10.08 μM	DMF	S13
16	$\{[Zn_6Cl_6(2,2'\text{-dbpt})_3]\cdot 4.5H_2O\}_n$	$Cr_2O_7^{2-}$	--	13.64 μM	DMF : H_2O	S15
17	CUST-605	$Cr_2O_7^{2-}$	60–350 μM	21.6 μM	DMF	S13
18	$\{[TbL(H_2O)]\cdot 2H_2O\}_n$	$Cr_2O_7^{2-}$	--	25.3 μM	H_2O	S16
19	$[Tb(ppda)(npdc)_{0.5}(H_2O)_2]_n$	$Cr_2O_7^{2-}$	--	60 μM	H_2O	S17
20	$\{[Cd(L)(bpe)_{0.5}]\cdot H_2O\}_n$	$Cr_2O_7^{2-}$	--	78.9 μM	H_2O	S18
21	**Complex 6**	**CrO_4^{2-}**	**0–1.45 μM**	**5.35 nM**	**H_2O**	**This work**
22	$[Tb_2(\mu_3\text{-}L)_2(\mu_4\text{-}L)(H_2O)_3]_n\cdot nH_2O$	CrO_4^{2-}	0–1.5 μM	40.6 nM	H_2O	S19
23	HBU-20	CrO_4^{2-}	--	65 nM	H_2O	S4
24	UiO-66-NH-BT	CrO_4^{2-}	--	0.411 μM	H_2O	S10
25	$[Tb(L)(HCOO)(H_2O)]_n$	CrO_4^{2-}	--	1.8 μM	H_2O	S11

26	$\{[Zn_6Cl_6(2,2'\text{-dbpt})_3]\cdot 4.5H_2O\}_n$	CrO_4^{2-}	--	12.33 μM	DMF : H_2O	S15
27	$\{[Cd(L)(bpe)_{0.5}]\cdot H_2O\}_n$	CrO_4^{2-}	--	92.1 μM	H_2O	S18
18	gC_3N_4–CdS	TC	0.01–0.25 μM	5.3 nM	Na_2SO_4	S20
19	Atta-CDs-Eu	TC	0–20 μM	8.7 nM	H_2O	S21
20	Laponite-Eu-Cit	TC	0–7 μM	9.5 nM	H_2O	S22
21	$[Cd(L)(SA)]_n$	TC	0–0.5 μM	33 nM	H_2O	S23
22	Eu-MOF	TC	0–140 μM	39.8 nM	H_2O	S24
23	$[Cd(L)(chdc)\cdot(H_2O)]_n$	TC	0–1.7 μM	76 nM	H_2O	S23
24	Eu^{3+}/NH_2-MIL-53(Al)	TC	0.5–60 μM	0.16 μM	Tris–HCl	S25
25	**Complex 6**	**TC**	**0–40 μM**	**0.24 μM**	**H_2O**	**This work**
26	In-sbdc	TC	--	0.28 μM	Tris–HCl	S26
27	Ag NCs	TC	1.12–230 μM	0.47 μM	BR buffer	S27
28	NH_2-MIL-53(Al)	TC	1.5–70 μM	0.92 μM	Tris–HCl	S25
29	ND-MS/GCE	TC	5–180 μM	2 μM	PBS buffer	S28
30	JLUE-MOGs	CTC	--	79 nM	H_2O	S29
31	Tb-L1	CTC	--	83 nM	H_2O	S30
32	CuNCs@TA	CTC	0.5–200 μM	84 nM	H_2O	S31
33	**Complex 6**	**CTC**	**0–25 μM**	**0.25 μM**	**H_2O**	**This work**
34	N-CDs	CTC	5–100 μM	0.254 μM	H_2O	S32
35	In-sbdc	CTC	--	0.30 μM	Tris–HCl	S26

Table S6 Quantum yield results of complex **6** after adding $Cr_2O_7^{2-}$, CrO_4^{2-}, CTC or TC

Sample	**6@$Cr_2O_7^{2-}$**	**6@CrO_4^{2-}**	**6@CTC**	**6@TC**
Quantum yield	22.6%	22.5%	23.9%	23.4%

Table S7. Resonance energy transfer efficiency of complex **6**. ($E = 1 - \tau_1 / \tau_0$, where τ_1 and τ_0 are the excited-state lifetime of $Cr_2O_7^{2-}$, CrO_4^{2-}, CTC or TC in the presence and absence of complex **6**)

Excited-state lifetime / ms	**τ_0**	**τ_1**	**Resonance energy transfer efficiency (E)**
6	1.097		
6@$Cr_2O_7^{2-}$		1.062	3.2%
6@CrO_4^{2-}		1.074	2.1%
6@CTC		1.081	1.5%
6@TC		1.084	1.2%

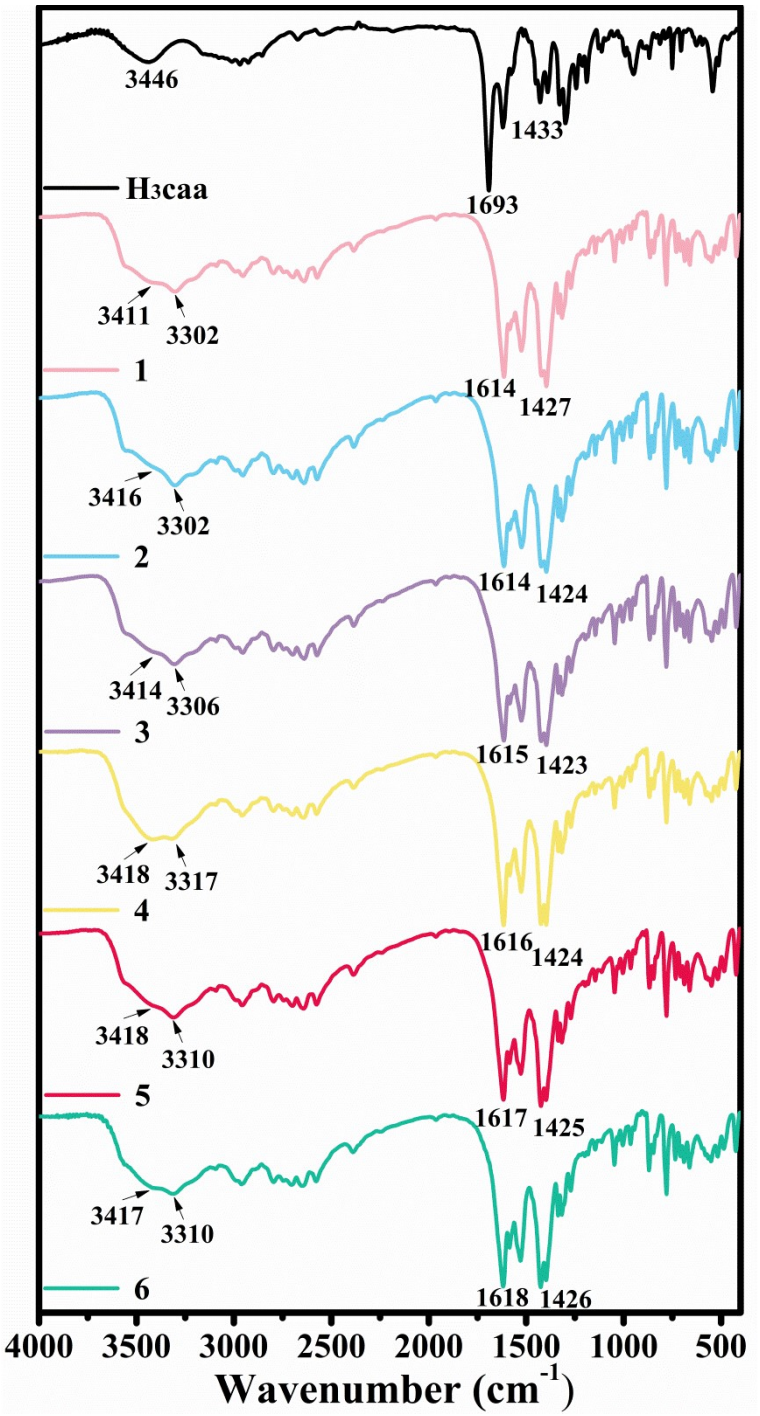

Fig. S1 IR spectra of ligand (H_3caa) and complexes **1** − **6** (KBr, cm^{-1})

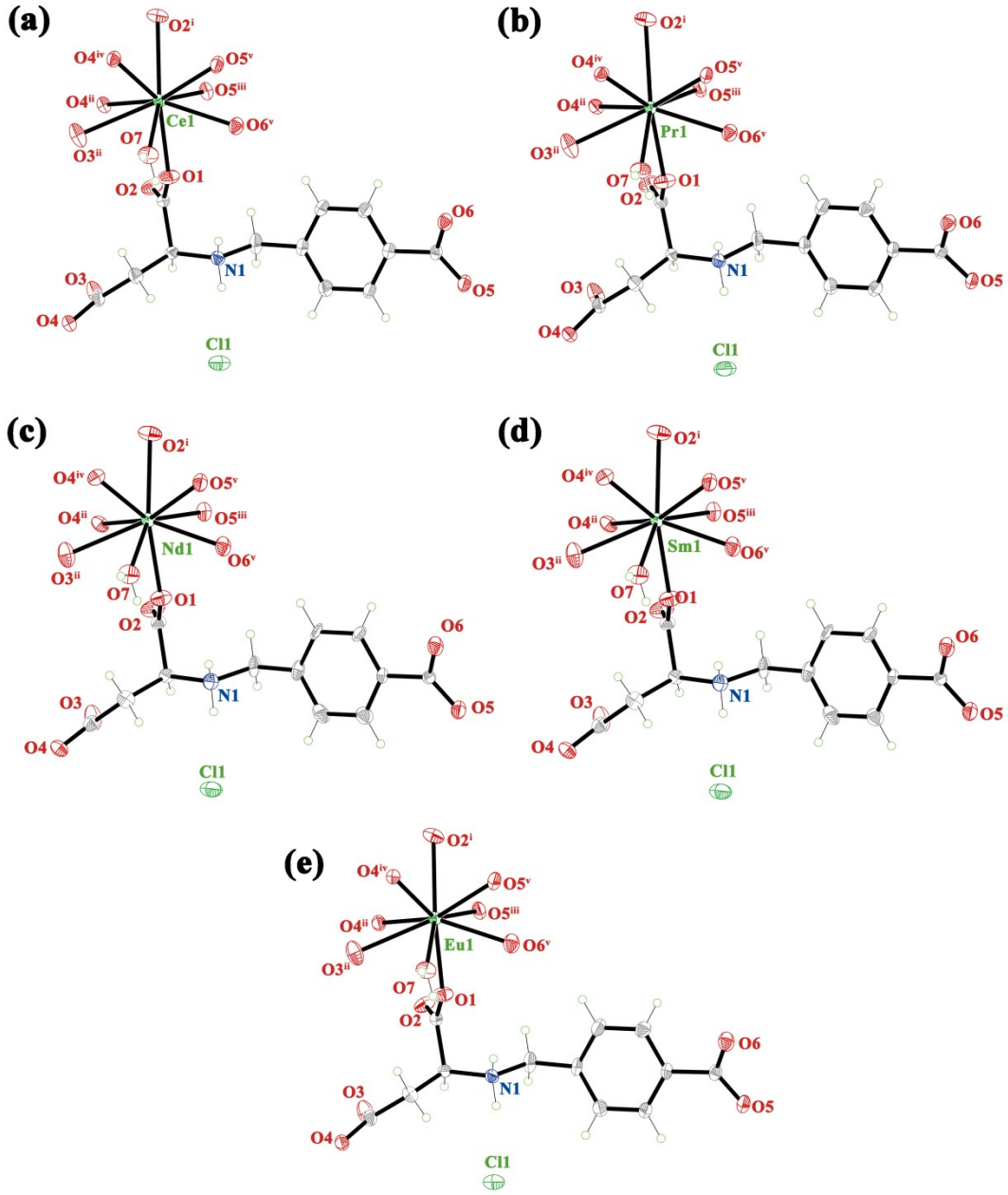

Fig. S2 Coordination environment diagrams of complexes **1 − 5**

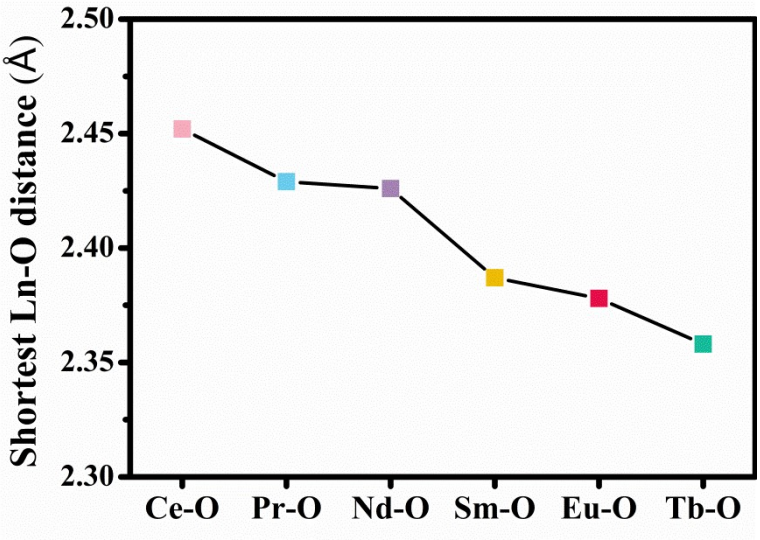

Fig. S3 The shortest Ln-O bond length of complexes **1** − **6**

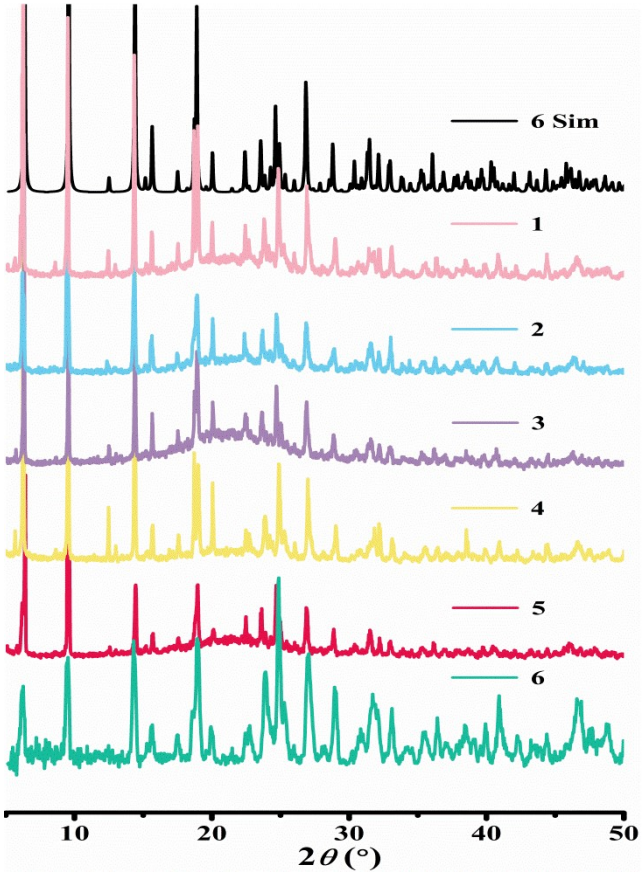

Fig. S4 PXRD patterns (simulated and experimental) for complexes **1** − **6** in the 2θ range of 5 to

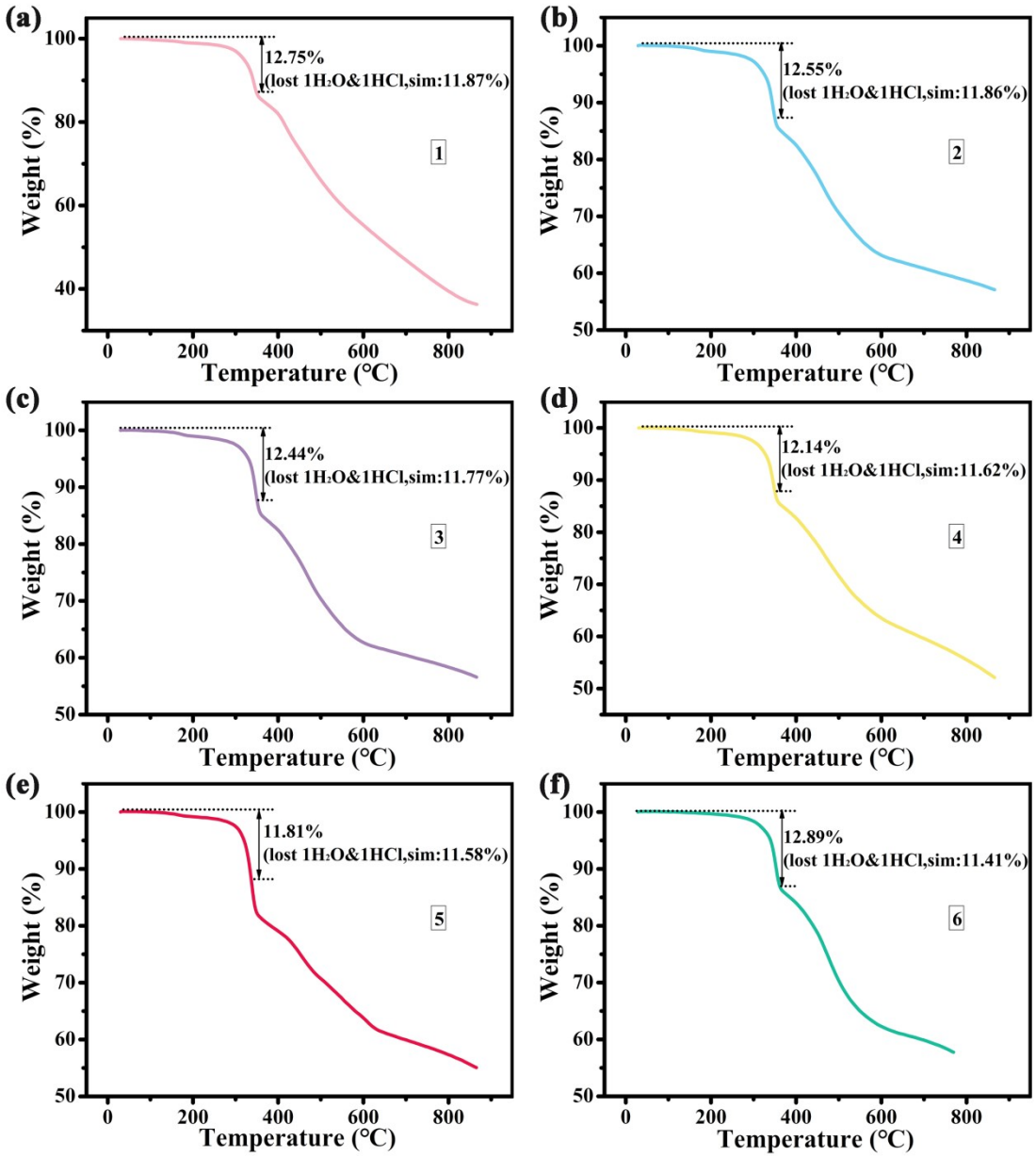

Fig. S5 TGA curves for complexes **1** − **6** collected under air atmosphere

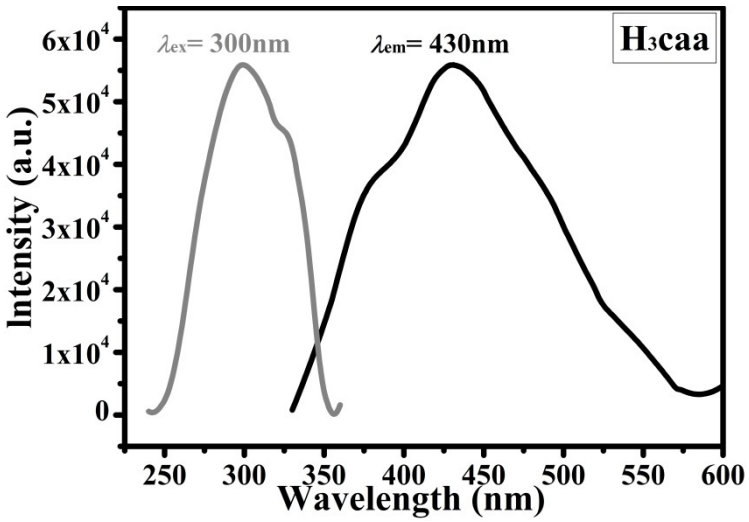

Fig. S6 Solid-state luminescent spectra of ligand (H_3caa)

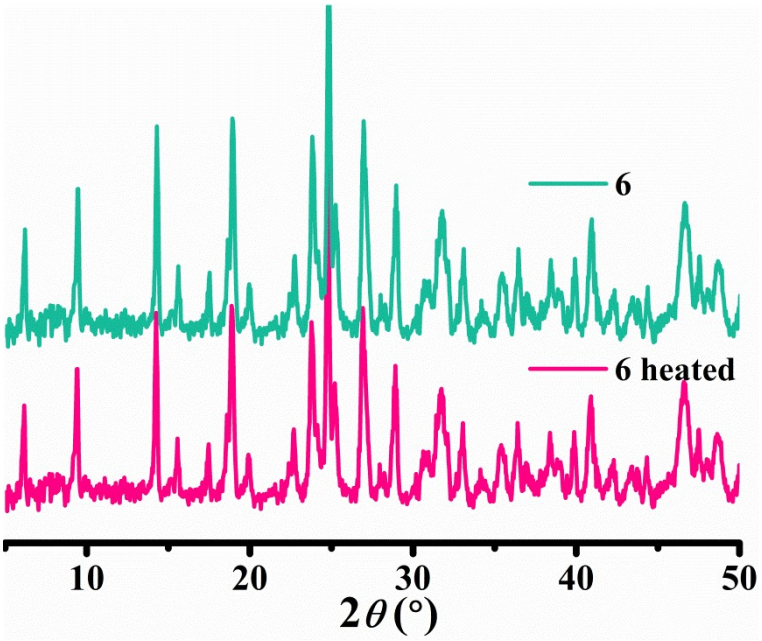

Fig. S7 PXRD patterns of complex **6** at room temperature (green) and after heating at 95ºC (pink)

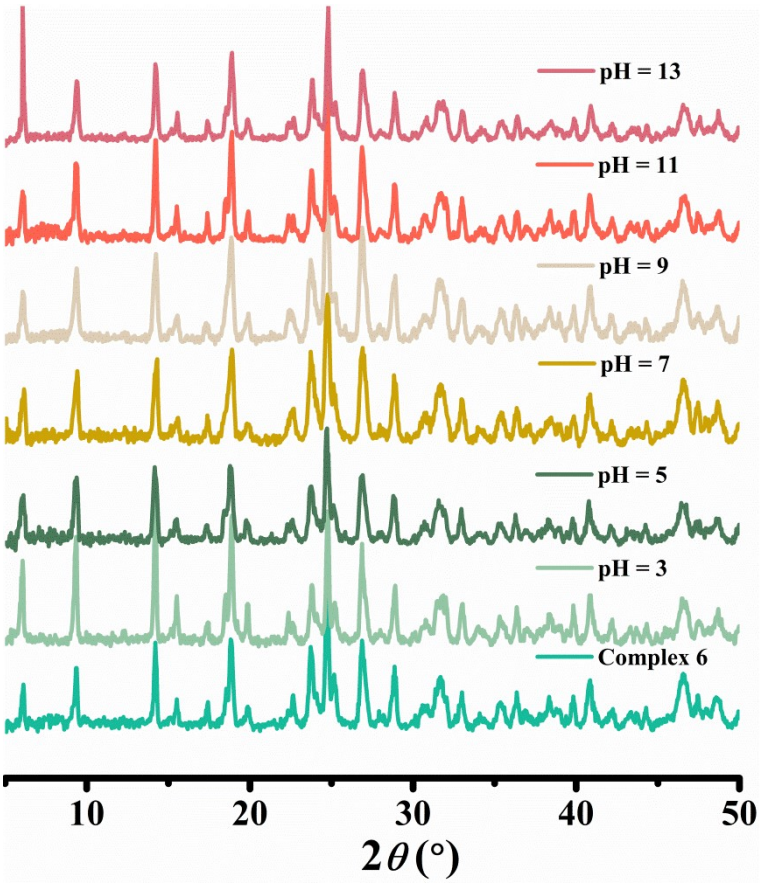

Fig. S8 PXRD patterns of complex **6** before (green) and after soaking in different pH = 3 – 13

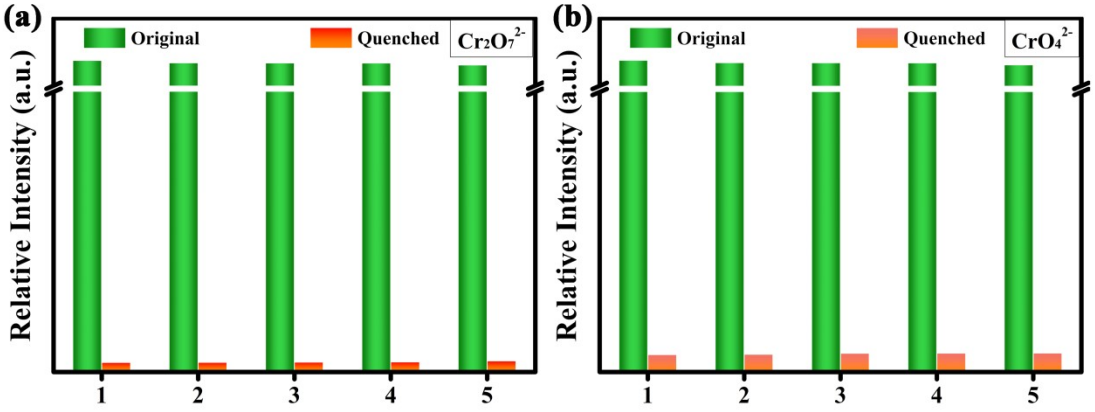

Fig. S9 Fluorescence intensity for the recognition of (a) $Cr_2O_7^{2-}$ or (b) CrO_4^{2-} after five cycles of isolation and re-suspending complex **6** in water

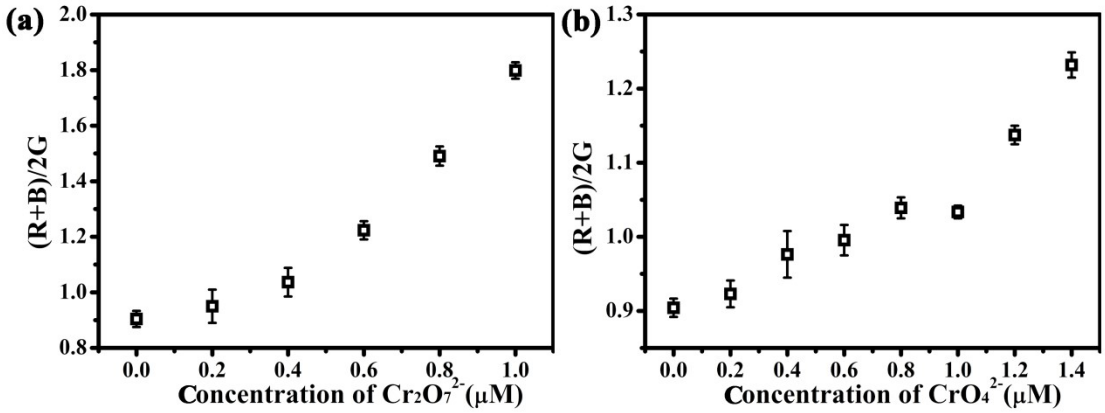

Fig. S10 Standard curves of (R + B) /2G formula to qualitatively analyse the strips of (a) $Cr_2O_7^{2-}$ or (b) CrO_4^{2-}

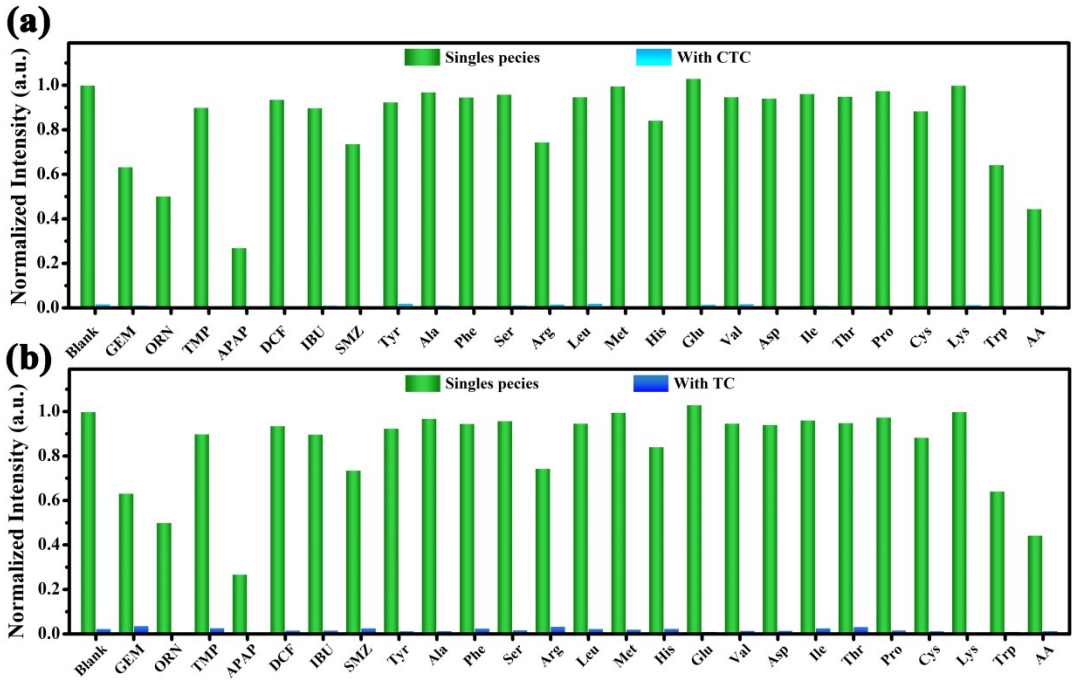

Fig. S11 Anti-interference of complex **6** to (a) CTC or (b) TC in the presence of other biomolecules at 543 nm

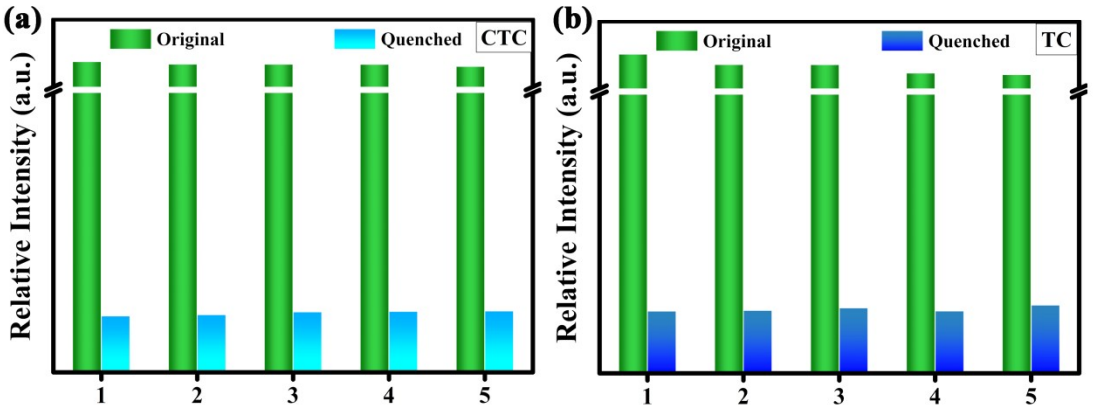

Fig. S12 Fluorescence intensity for the recognition of (a) CTC or (b) TC after five cycles of isolation and re-suspending complex **6** in water

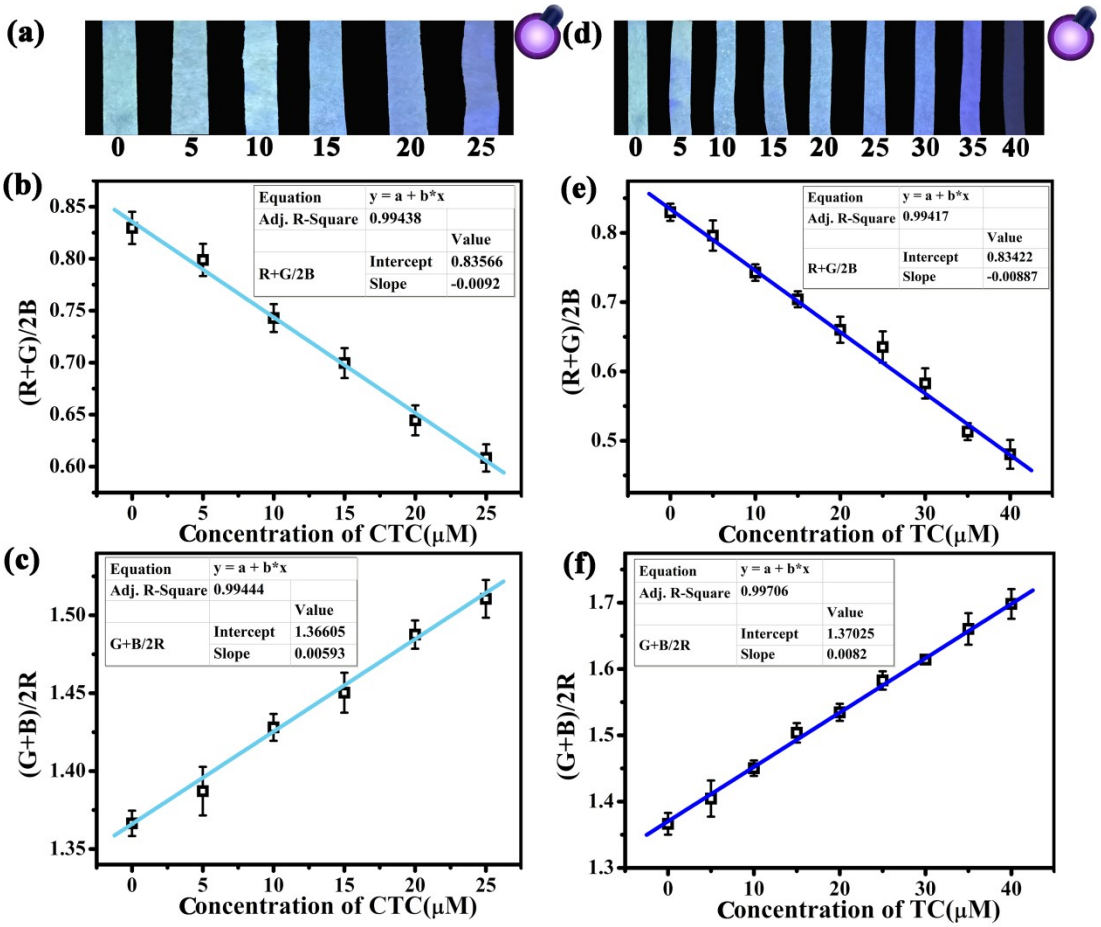

Fig. S13 Color changes of complex **6** strips for detecting (a) CTC (0 ~ 25 μM) or (d) TC (0 ~ 40 μM). The standard curves of (b, e) (R + G) /2B formula and (c, f) (G + B) /2R formula to qualitatively analyse the strip

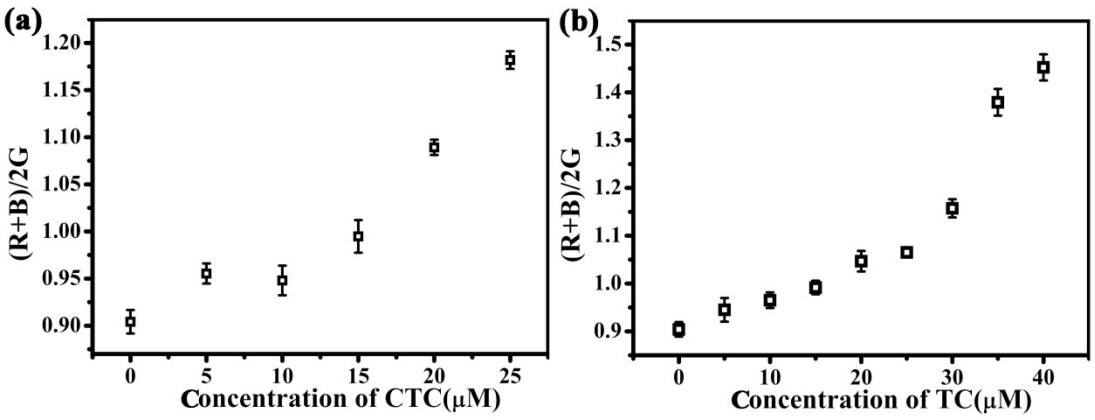

Fig. S14 Standard curves of (R + B) /2G formula to qualitatively analyse the strips of (a) CTC or (b) TC

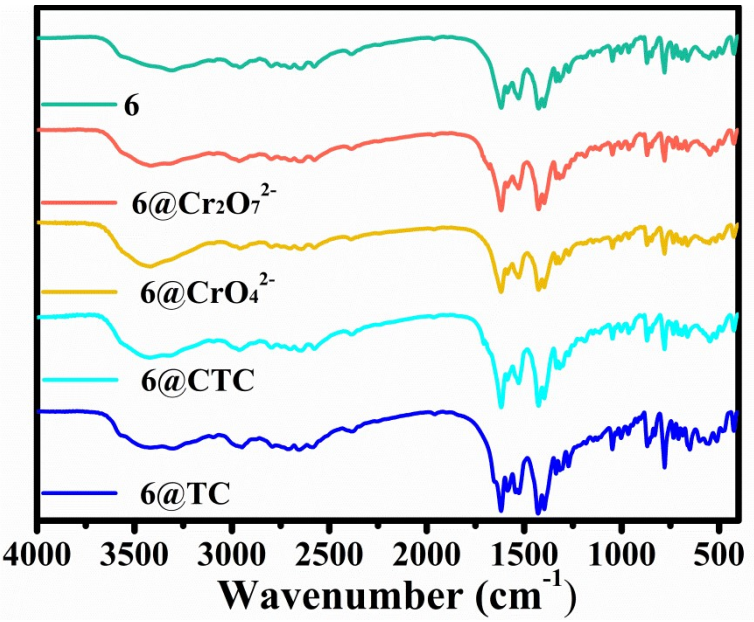

Fig. S15 IR spectra of complex **6** before and after soaking in $Cr_2O_7^{2-}$, CrO_4^{2-}, CTC or TC for 7 days

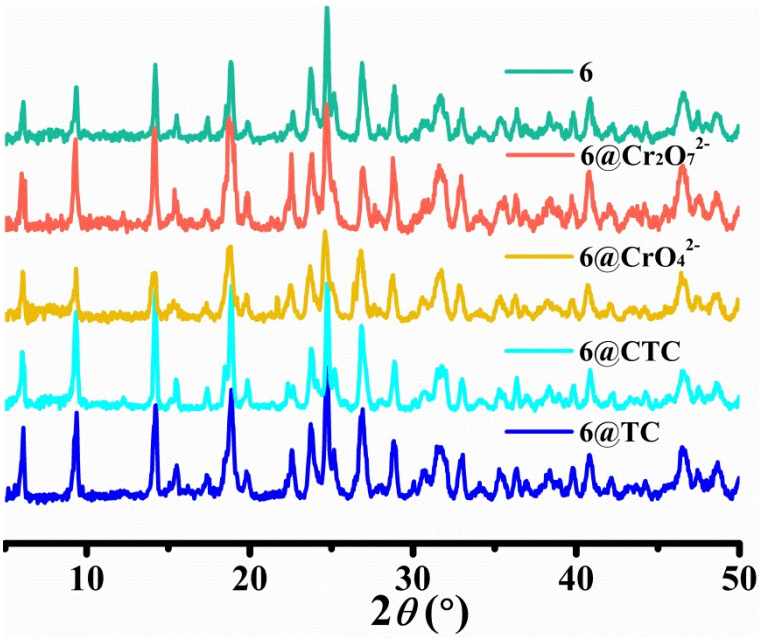

Fig. S16 PXRD patterns of complex **6** before and after soaking in $Cr_2O_7^{2-}$, CrO_4^{2-}, CTC or TC for 7 days

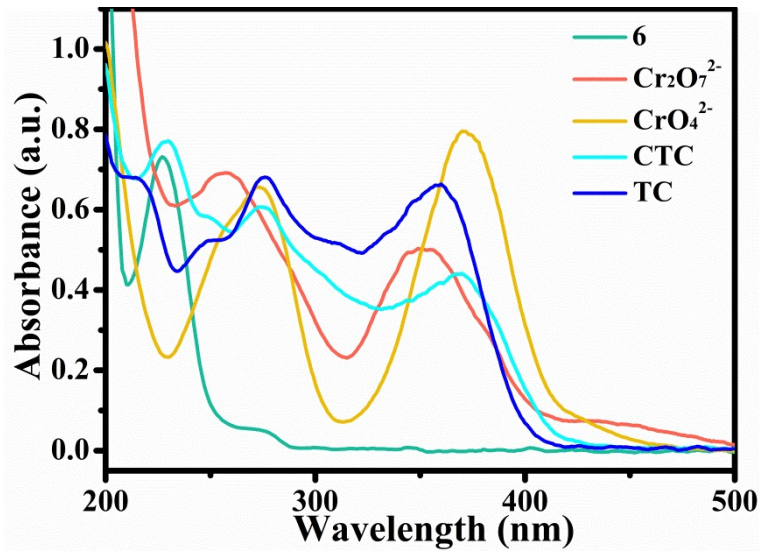

Fig. S17 Liquid UV-vis spectra of complex **6,** $Cr_2O_7^{2-}$, CrO_4^{2-}, CTC and TC in the aqueous solution

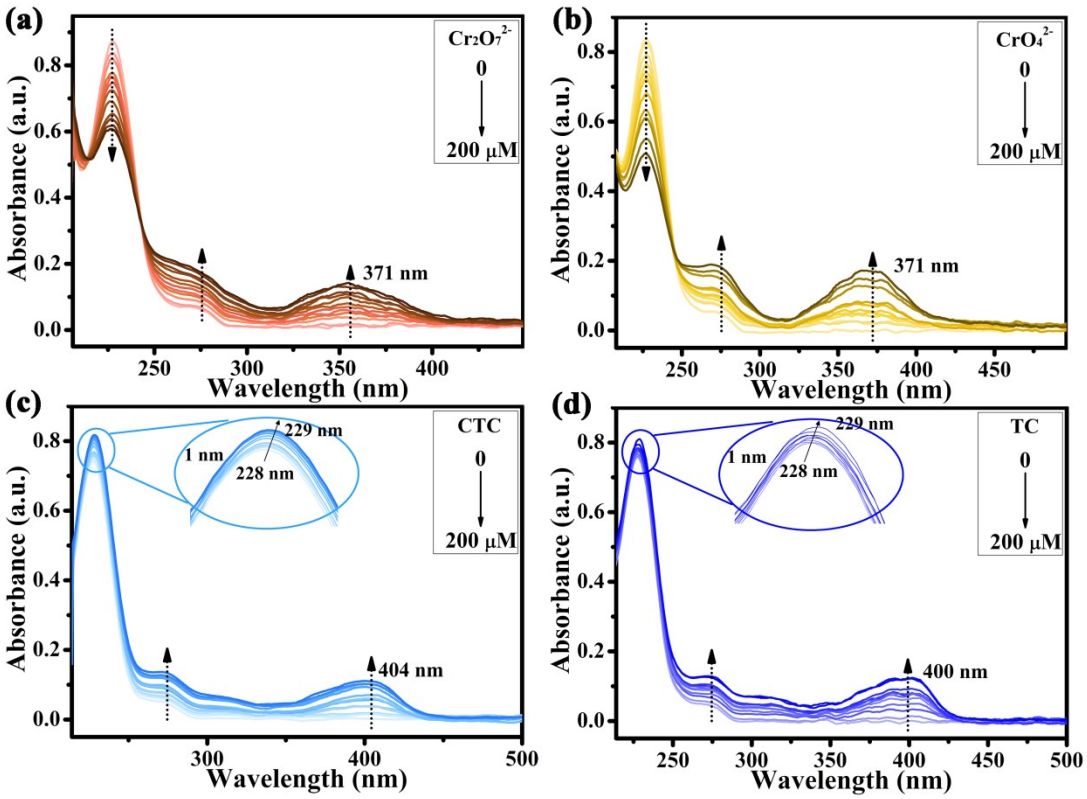

Fig. S18 Liquid UV-vis spectra of complex **6** with the addition of different concentrations of $Cr_2O_7^{2-}$, CrO_4^{2-}, CTC or TC

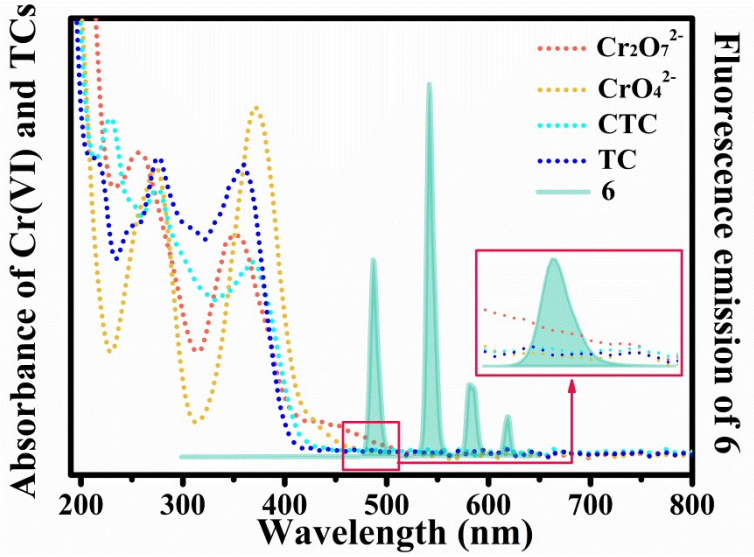

Fig. S19 Emission spectrum of complex **6** and the absorption spectra of $Cr_2O_7^{2-}$, CrO_4^{2-}, CTC and TC

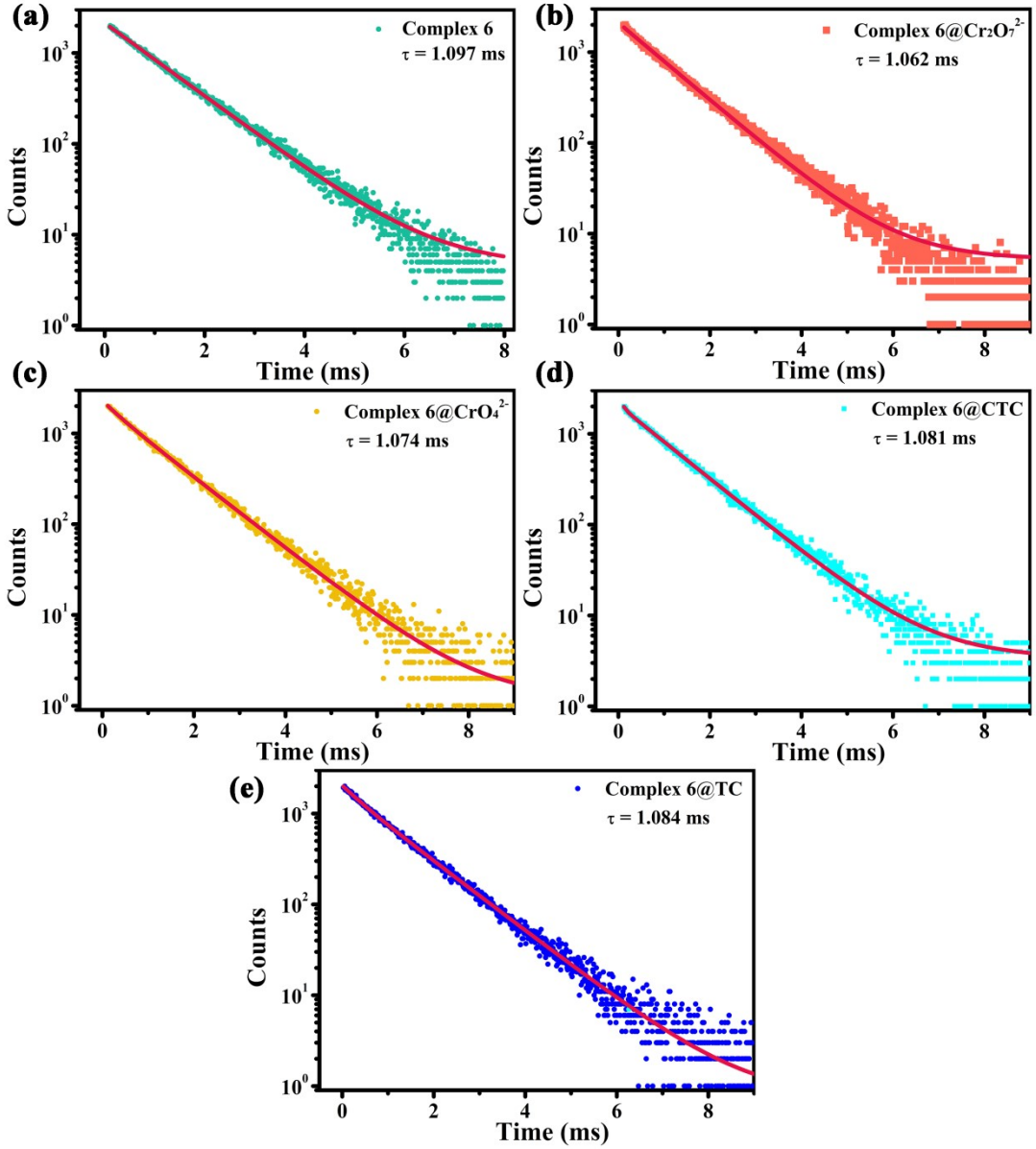

Fig. S20 Photoluminescence decay times of complex **6** before and after loading in $Cr_2O_7^{2-}$, CrO_4^{2-}, CTC or TC

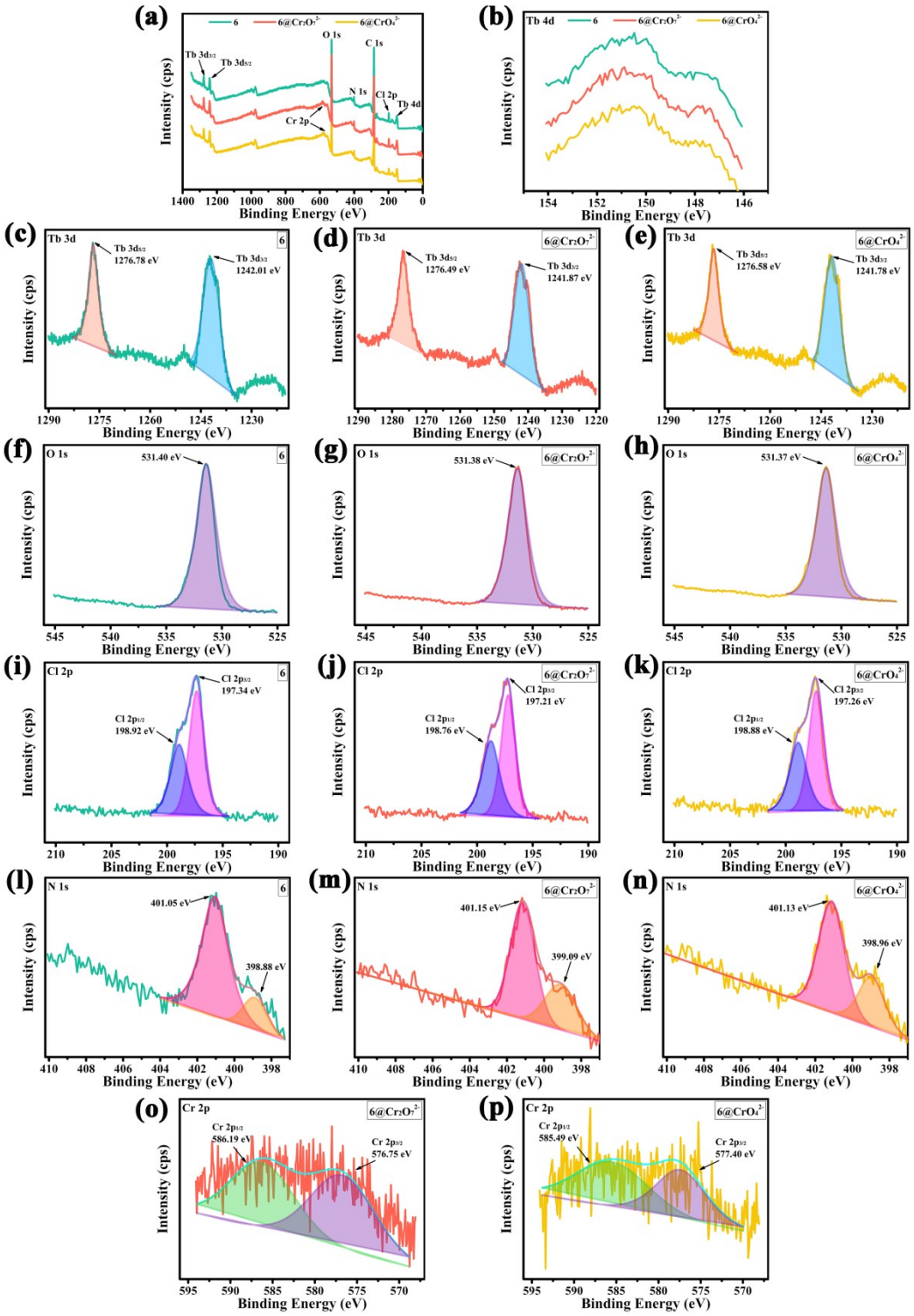

Fig. S21 XPS spectra of complex **6** before and after loading in $Cr_2O_7^{2-}$ or CrO_4^{2-}

References

S1. Bruker (2014). *XPREP* (Version 2014/2) and *SADABS* (Version 2014/4). Bruker AXS Inc., Madison, Wisconsin, USA.

S2. Sheldrick, G. A short history of SHELX, Acta Crystallographica Section A 2008; 64: 112–122.

S3. Price, J.; Balonova, B.; Blight, B. A.; Eisler, S., Shedding light on predicting and controlling emission chromaticity in multicomponent photoluminescent systems. Chem. Sci 2021, 12, 12092.

S4. Ren, Y. B.; Xu, H. Y.; Yan, J. W.; Cao, D. X.; Du, J. L., Multifunctional luminescent Zr(IV)-MOF for rapid and efficient detection of vanillin, CrO_4^{2-} and $Cr_2O_7^{2-}$ ions. Spectrochim Acta A Mol Biomol Spectrosc 2022, 278, 121390.

S5. Chen, W.; Fan, R.; Fan, J.; Liu, H.; Sun, T.; Wang, P.; Yang, Y., Lanthanide Coordination Polymer-Based Composite Films for Selective and Highly Sensitive Detection of $Cr_2O_7^{2-}$ in Aqueous Media. Inorg Chem 2019, 58 (22), 15118-15125.

S6. Zhang, J.; Liu, J.; Li, X.; Xu, Y., Solvent-free synthesis of hierarchical Tb^{3+}-doped Yttrium benzene-1,3,5-tricarboxylate metal organic framework nanosheets for fast and highly sensitive fluorescence detection of Fe^{3+} and $Cr_2O_7^{2-}$ ions. Resources Chemicals and Materials 2022, 1 (2), 146-151.

S7. Gao, T.; Ren, Y.; Wang, Z.; Zhang, M.; Cao, J.; Wang, J., A multi-functional Tb-organic network featuring high selectivity fluorescent sensing for Fe^{3+}, $Cr_2O_7^{2-}$, tetracycline and 2,4,6-trinitrophenol in aqueous solution. Journal of Solid State Chemistry 2022, 309.

S8. Yin, J.; Chu, H.; Qin, S.; Qi, H.; Hu, M., Preparation of $Eu_{0.075}Tb_{0.925}$-Metal Organic Framework as a Fluorescent Probe and Application in the Detection of Fe^{3+} and $Cr_2O_7^{2-}$. Sensors (Basel) 2021, 21 (21).

S9. Sheng, D.; Sun, F.; Yu, Y. e.; Wang, Y.; Lu, J.; Li, Y.; Wang, S.; Dou, J.; Li, D., 1-D multifunctional Ln-CPs: Luminescence probes for Fe^{3+} and Cr(VI) and uncommon discriminative detection between $Cr_2O_7^{2-}$ and CrO_4^{2-} of Tb-CP in various media. Journal of Luminescence 2019, 213, 140-150.

S10. Helal, A.; Nasiruzzaman Shaikh, M.; Abdul Aziz, M., Dual sensing of copper ion and chromium (VI) oxyanions by benzotriazole functionalized UiO-66 metal-organic framework in aqueous media. Journal of Photochemistry and Photobiology A: Chemistry 2020, 389.

S11. Sun, Z.; Yang, M.; Ma, Y.; Li, L., Multi-Responsive Luminescent Sensors Based on Two-Dimensional Lanthanide–Metal Organic Frameworks for Highly Selective and Sensitive Detection of Cr(III) and Cr(VI) Ions and Benzaldehyde. Crystal Growth & Design 2017, 17 (8), 4326-4335.

S12. Liu, J.; Liu, S.; Ma, J.; Diao, Y.; Li, M.; He, J.; Chen, S.; Zhang, Q., A Stable 2D Zr(IV)-Based Metal-Organic Framework (USTS-7) for Selective Sensing of $Cr_2O_7^{2-}$ in Aqueous Solution. Inorg Chem 2020, 59 (24), 17884-17888.

S13. Li, J.; Tian, J.; Yu, H.; Fan, M.; Li, X.; Liu, F.; Sun, J.; Su, Z., Controllable Synthesis of Metal–Organic Frameworks Based on Anthracene Ligands for High-Sensitivity Fluorescence Sensing of Fe^{3+}, $Cr_2O_7^{2-}$, and TNP. Crystal Growth & Design 2022, 22 (5), 2954-2963.

S14. Li, J.; Xiao, Y.; Wang, L.; Xing, Y.; Bai, F.; Shi, Z., Oriented construction of the Mixed-metal organic framework with triazine hexacarboxylic acid and fluorescence detection: Fe^{3+}, $Cr_2O_7^{2-}$ and TNP. Polyhedron 2022, 214.

S15. Cao, Y.; Zhang, Y.; Gu, L.; Qin, X.; Li, H.; Bian, H.; Huang, F., A $zinc^{2+}$-dpbt framework: luminescence sensing of Cu^{2+}, Ag^{+}, MnO_4^{-} and Cr(vi) ($Cr_2O_7^{2-}$ and CrO_4^{2-}) ions. New Journal of Chemistry 2020, 44 (25), 10681-10688.

S16. Guo, F.; Chu, Z.; Zhao, M.; Zhu, B.; Zhang, X., A dual-responsive luminescent TbIII-organic framework with high water stability for selective sensing of Fe^{3+} and $Cr_2O_7^{2-}$ in water systems. Inorganic Chemistry Communications 2019, 104, 71-77.

S17. Li, Z.; Zhan, Z.; Hu, M., A luminescent terbium coordination polymer as a multifunctional water-stable sensor for detection of Pb^{2+} ions, PO_4^{3-} ions, $Cr_2O_7^{2-}$ ions, and some amino acids. CrystEngComm 2020, 22 (40), 6727-6737.

S18. Xi, W. K.; Ma, G.; Wang, X. G.; Sun, Z. H.; Li, J.; Zhang, L., A multifunctional 3D Cd-based metal-organic frameworks for the highly luminescence sensitive detection of CrO_4^{2-} / $Cr_2O_7^{2-}$ and nitro aromatic compounds. Polyhedron 2020, 188.

S19. Wei, W.; Zhang, X.; Lu, L.; Feng, S., Novel 2D isomorphic lanthanide complexes based on a bifunctional 5-(pyridin-3-yloxy)isophthalic acid: synthesis, structure, fluorescence and magnetic properties. CrystEngComm 2022, 24 (35), 6204-

6214.

S20. Liu, Y.; Yan, K.; Zhang, J., Graphitic Carbon Nitride Sensitized with CdS Quantum Dots for Visible-Light-Driven Photoelectrochemical Aptasensing of Tetracycline. ACS Appl Mater Interfaces 2016, 8 (42), 28255-28264.

S21. Jia, L.; Chen, R.; Xu, J.; Zhang, L.; Chen, X.; Bi, N.; Gou, J.; Zhao, T., A stick-like intelligent multicolor nano-sensor for the detection of tetracycline: The integration of nano-clay and carbon dots. J Hazard Mater 2021, 413, 125296.

S22. Xu, J.; Guo, S.; Jia, L.; Zhu, T.; Chen, X.; Zhao, T., A smartphone-integrated method for visual detection of tetracycline. Chemical Engineering Journal 2021, 416.

S23. Cao, Q. L.; Wang, R. T.; Duan, J. Y.; Dong, G. Y., Two stable cadmium(II) coordination polymers for fluorimetric detection of tetracycline and Fe3+ ions. Journal of Solid State Chemistry 2022, 307.

S24. Gan, Z.; Hu, X.; Xu, X.; Zhang, W.; Zou, X.; Shi, J.; Zheng, K.; Arslan, M., A portable test strip based on fluorescent europium-based metal-organic framework for rapid and visual detection of tetracycline in food samples. Food Chem 2021, 354, 129501.

S25. Chen, J.; Xu, Y.; Li, S.; Xu, F.; Zhang, Q., Ratio fluorescence detection of tetracycline by a Eu^{3+}/NH_2-MIL-53(Al) composite. RSC Adv 2021, 11 (4), 2397-2404.

S26. Liu, Q.; Ning, D.; Li, W. J.; Du, X. M.; Wang, Q.; Li, Y.; Ruan, W. J., Metal-organic framework-based fluorescent sensing of tetracycline-type antibiotics applicable to environmental and food analysis. Analyst 2019, 144 (6), 1916-1922.

S27. Zhang, Y.; Lv, M.; Gao, P.; Zhang, G.; Shi, L.; Yuan, M.; Shuang, S., The synthesis of high bright silver nanoclusters with aggregation-induced emission for detection of tetracycline. Sensors and Actuators B: Chemical 2021, 326.

S28. Fernandes-Junior, W. S.; Zaccarin, L. F.; Oliveira, G. G.; de Oliveira, P. R.; Kalinke, C.; Bonacin, J. A.; Prakash, J.; Janegitz, B. C.; Srivastava, S. K., Electrochemical Sensor Based on Nanodiamonds and Manioc Starch for Detection of Tetracycline. Journal of Sensors 2021, 2021, 1-10.

S29. Liu, M.; Xia, S.; Liu, Z.; Ma, T.; Liu, Z.; Li, Y.; Zou, D., Luminescent porous

metal–organic gels for efficient adsorption and sensitive detection of chlortetracycline hydrochloride assisted by smartphones and a test paper-based analytical device. Inorganic Chemistry Frontiers 2022, 9 (8), 1722-1734.

S30. Li, R.; Wang, W.; El-Sayed, E. S. M.; Su, K.; He, P.; Yuan, D., Ratiometric fluorescence detection of tetracycline antibiotic based on a polynuclear lanthanide metal–organic framework. Sensors and Actuators B: Chemical 2021, 330.

S31. Guo, Y.; Hu, Y..; Chen, S; Guo, M.; Zhang, Y.; Han, X.; Zhang, S., Facile one-pot synthesis of tannic acid-stabilized fluorescent copper nanoclusters and its application as sensing probes for chlortetracycline based on inner filter effect. Colloids and Surfaces A: Physicochemical and Engineering Aspects 2022, 634.

S32. Zhang, W.; Li, X.; Liu, Q.; Liu, G.; Yue, G.; Yang, Z.; Wang, Y.; Rao, H.; Chen, Y.; Lu, C.; Wang, X., Nitrogen-doped carbon dots from rhizobium as fluorescence probes for chlortetracycline hydrochloride. Nanotechnology 2020, 31 (44), 445501.